

Article

Synthesis of Silver-Strontium Titanate Hybrid Nanoparticles by Sol-Gel-Hydrothermal Method

Shintaro Ueno *, Kouichi Nakashima, Yasunao Sakamoto and Satoshi Wada

Graduate School Department of Interdisciplinary Research, University of Yamanashi, 4-4-37 Takeda, Kofu 400-8510, Japan; E-Mails: knakashima@yamanashi.ac.jp (K.N.); g14ma018@yamanashi.ac.jp (Y.S.); swada@yamanashi.ac.jp (S.W.)

* Author to whom correspondence should be addressed; E-Mail: sueno@yamanashi.ac.jp; Tel.: +81-55-220-8545.

Academic Editor: Thomas Nann

Received: 4 February 2015 / Accepted: 18 March 2015 / Published: 24 March 2015

Abstract: Silver (Ag) nanoparticle-loaded strontium titanate (SrTiO₃) nanoparticles were attempted to be synthesized by a sol-gel-hydrothermal method. We prepared the titanium oxide precursor gels incorporated with Ag⁺ and Sr²⁺ ions with various molar ratios, and they were successfully converted into the Ag-SrTiO₃ hybrid nanoparticles by the hydrothermal treatment at 230 °C in strontium hydroxide aqueous solutions. The morphology of the SrTiO₃ nanoparticles is dendritic in the presence and absence of Ag⁺ ions. The precursor gels, which act as the high reactive precursor, give rise to high nucleation and growth rates under the hydrothermal conditions, and the resultant diffusion-limited aggregation phenomena facilitate the dendritic growth of SrTiO₃. From the field-emission transmission electron microscope observation of these Ag-SrTiO₃ hybrid nanoparticles, the Ag nanoparticles with a size of a few tens of nanometers are distributed without severe agglomeration, owing to the competitive formation reactions of Ag and SrTiO₃.

Keywords: silver nanoparticles; strontium titanate; sol-gel-hydrothermal method; hybrid particles

1. Introduction

The sol-gel method is well-known as one of the versatile methods to synthesize inorganic compounds, including metal oxides, complex oxides, chalcogenides, and so on. This method is a promising low-energy method; however, in the case of powder syntheses, a subsequent heating process is frequently needed to obtain the desired compounds, and agglomerated nanoparticles are usually obtained. On the other hand, the sol-gel method combined with a hydrothermal method, the sol-gel-hydrothermal method, is capable of synthesizing microstructure-controlled nanoparticles at a lower temperature. There are many reports on the synthesis of various kinds of functional oxides by the sol-gel-hydrothermal method [1,2]. Among them, we are especially interested in the synthesis of perovskite oxides with unique morphologies by the sol-gel-hydrothermal method, such as barium titanate (BaTiO_3) nanoparticles [3], BaTiO_3 hollow nanoparticles [4], BaTiO_3 thin films [5], strontium titanate (SrTiO_3) nanocubes [6] and sodium-potassium bismuth titanate ($(\text{Na}_{0.8}\text{K}_{0.2})_{0.5}\text{Bi}_{0.5}\text{TiO}_3$) nanowires [7]. These morphologies of the perovskite oxides synthesized by the sol-gel-hydrothermal method are frequently different from those obtained by the hydrothermal method [8,9].

We attempt to apply the sol-gel-hydrothermal method for a synthesis of metal-complex oxide hybrid materials, especially metal nanoparticle-loaded oxide materials, which are expected to be applied to multi-functional materials. For example, the various kinds of metal nanoparticle-loaded perovskite oxide hybrid particles were attempted to be applied to photocatalysts [10–14]. For the synthesis of such nanometer-scale hybrid particles, the sol-gel-hydrothermal method is considered to be appropriate, because relatively high-crystallinity materials can be obtained at low temperature and oxidization or the grain growth of metal particles can be suppressed. Moreover, the size and morphology of hybrid particles are able to be controlled by modifying the synthesis conditions.

In our previous report, we synthesized Ag-BaTiO_3 hybrid particles by the sol-gel-hydrothermal method to fabricate Ag/BaTiO_3 nanocomposite compacts for capacitor applications [15]. Such metal/insulator composite capacitors with distributed metal particles in the insulator layer have attracted much attention because of their extremely high capacitance over 10^4 [16–19], and the distribution state of the metal particles is required to be precisely controlled, that is the metal particles should be insulated by the insulator layer and homogeneously distributed to enhance the dielectric breakdown strength. The metal-insulator hybrid particles are helpful for enhancing the distribution of the metal nanoparticles. The metal nanoparticles are fixed on the surface of the larger insulator particles, and thus, the aggregation of metal nanoparticles can be suppressed. Actually, by using the Ag-BaTiO_3 hybrid particles as the component, the resistivity of the Ag/BaTiO_3 nanocomposite materials was enhanced.

In this study, for the fabrication of the metal/paraelectric nanocomposite capacitors, Ag nanoparticle-loaded SrTiO_3 hybrid particles were attempted to be synthesized from amorphous titanium oxide gels incorporated with Ag^+ ions by the sol-gel-hydrothermal method. We prepared the precursor gels by mixing the Ag , Sr and Ti sources in various molar ratios, and the size and morphology of the synthesized hybrid particles were investigated.

2. Results and Discussion

2.1. Preparation of Precursor Gels

Precursor gels were prepared by mixing and drying silver acetate (CH_3COOAg) and strontium acetate hemihydrate ($\text{Sr}(\text{CH}_3\text{COO})_2 \cdot 0.5\text{H}_2\text{O}$) mixed aqueous solution and titanium tetraisopropoxide ($\text{Ti}[(\text{CH}_3)_2\text{CHO}]_4$) ethanolic solution. Figure 1 shows the X-ray diffraction (XRD) patterns of the precursor gels before the hydrothermal treatment. The XRD patterns of the precursor gels with molar ratios of Ag:Sr:Ti = 1:0:4 and 1:1:4 in Figure 1a,b show an amorphous pattern, while the XRD peaks identified as $\text{Sr}(\text{CH}_3\text{COO})_2 \cdot 0.5\text{H}_2\text{O}$ are found for the XRD patterns of the precursor gels with molar ratios of Ag:Sr:Ti = 1:2:4, 1:3:4 and 1:4:4 (Figure 1c,d,f). Since there is no peak identified as CH_3COOAg for these precursor gels regardless of the Sr molar fractions, Ag^+ ions are assumed to be preferentially incorporated into amorphous titanium oxide gel networks. In the case of the lower Sr molar fractions, Sr^{2+} ions are completely incorporated into the amorphous gel networks with Ag^+ ions. However, for the higher Sr molar fractions (molar ratios of Ag:Sr:Ti = 1:3:4 and 1:4:4), excess $\text{Sr}(\text{CH}_3\text{COO})_2 \cdot 0.5\text{H}_2\text{O}$ crystals were precipitated. On the other hand, XRD patterns of the series of precursor gels with the various Ag molar fractions (the molar ratio of Sr:Ti was fixed to 1:1) are shown in Figure 1e–h. All of the XRD peaks are identified as $\text{Sr}(\text{CH}_3\text{COO})_2 \cdot 0.5\text{H}_2\text{O}$ for the precursor gels with molar ratios of Ag:Sr:Ti = 0:4:4, 1:4:4 and 2:4:4 (Figure 1e–g). In contrast, other than the $\text{Sr}(\text{CH}_3\text{COO})_2 \cdot 0.5\text{H}_2\text{O}$ peaks, the peaks identified as CH_3COOAg are found for the precursor gel with a molar ratio of Ag:Sr:Ti = 4:4:4 (Figure 1h). Therefore, Ag^+ ions are completely incorporated into the gel networks for the precursor gels with the lower Ag molar fractions (molar ratios of Ag:Sr:Ti = 1:4:4 and 2:4:4). For these precursor gels, a certain amount of Ag^+ and Sr^{2+} ions are incorporated into the amorphous titanium oxide gel networks, and excesses of $\text{Sr}(\text{CH}_3\text{COO})_2 \cdot 0.5\text{H}_2\text{O}$ and CH_3COOAg are precipitated.

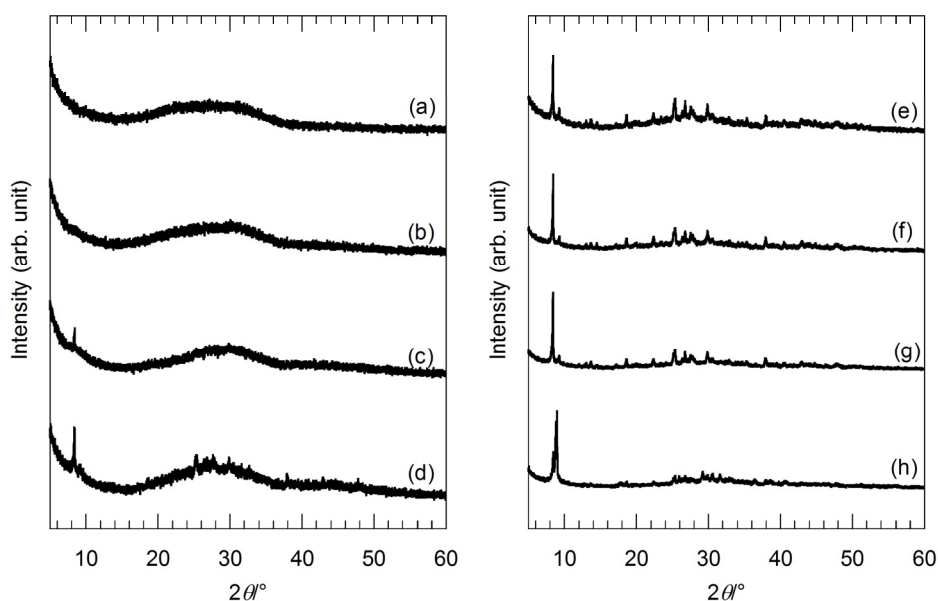


Figure 1. X-ray diffraction (XRD) patterns of the precursor gels with various molar ratios of (a) Ag:Sr:Ti = 1:0:4; (b) 1:1:4; (c) 1:2:4; (d) 1:3:4; (e) 0:4:4; (f) 1:4:4; (g) 2:4:4; and (h) 4:4:4.

2.2. Synthesis of Hybrid Particles from Precursor Gels with Various Sr Molar Fractions

Figure 2 shows XRD patterns of the hybrid particles synthesized from the precursor gels with molar ratios of Ag:Sr:Ti = 1:0:4, 1:2:4, 1:3:4 and 1:4:4 by the hydrothermal treatment in strontium hydroxide ($\text{Sr}(\text{OH})_2$) aqueous solutions. The hydrothermally-synthesized sample powder from the precursor gel without Sr^{2+} ion (Ag:Sr:Ti = 1:0:4), which was reacted with $\text{Sr}(\text{OH})_2$, mainly consists of Ag and SrTiO_3 , though this sample contains impurities; anatase- and rutile-type TiO_2 (Figure 2a). When the other precursor gels containing Sr^{2+} ions were used, we could obtain the Ag- SrTiO_3 hybrid particles without impurity (Figure 2b–e), because the Sr source included in the precursor gels relatively increases and the Ti source included in the gels relatively decreases. In the hydrothermal reaction, the Sr^{2+} ions dissociated from the gel networks, and the excess $\text{Sr}(\text{CH}_3\text{COO})_2 \cdot 0.5\text{H}_2\text{O}$ could be also reacted with titanium oxide gels other than Sr^{2+} ions supplied by $\text{Sr}(\text{OH})_2$. Thus, the formation reaction of SrTiO_3 is considered to be facilitated for the precursor gels with the higher Sr molar fractions. In Figure 2, the XRD peaks originating from Ag tend to broaden with a decrease in the Ag molar fraction in the precursor gels. This suggests that the size of Ag nanoparticles becomes smaller by using the gels with the lower Ag molar fractions, because of a decrease in the supply of the Ag source. A comparison of the XRD peaks indexed as (110) of SrTiO_3 reveals a slight diffraction peak-shift. All of the XRD peaks originating from SrTiO_3 of the hybrid particles synthesized from the gels containing Sr^{2+} ions (Figure 2b–e) slightly shift toward a lower 2θ angle as compared to the hybrid particles from the precursor gel without Sr^{2+} ions (Figure 2a). Ag^+ ions can be doped into SrTiO_3 , because the Ag^+ ion radius is comparable to the Sr^{2+} ion radius [20]. However, it is difficult to confirm the doping of Ag^+ by the XRD measurement due to the similarity of the ion radii. For the case of BaTiO_3 particles synthesized by the hydrothermal method, it was reported that an incorporation of hydroxyl ions in the crystal lattice enlarges the cell volume [21–24]. Therefore, we investigated the presence of the hydroxyl defects in the synthesized SrTiO_3 crystals by a thermogravimetric analysis.

Figure 3 shows thermogravimetry-differential thermal analysis (TG-DTA) curves of the hybrid particles synthesized from the precursor gels with molar ratios of Ag:Sr:Ti = 1:0:4, 1:1:4, 1:2:4, 1:3:4 and 1:4:4 via the hydrothermal treatment at 230 °C for 6 h in $\text{Sr}(\text{OH})_2$ aqueous solutions. The weight loss is up to approximately 2.5%, and these hybrid particles are considered to contain a small amount of hydroxyl groups. The slight weight loss accompanied by the sharp exothermic peak is found at approximately 180 °C for all of the hybrid particles. The weight loss of the hybrid particles synthesized by the hydrothermal treatment in a range from 200 to 700 °C, which may be attributed to the hydroxyl ions incorporated in the SrTiO_3 crystals, monotonically increases from 1.1% to 1.9% with the Sr molar fraction in the precursor gels. Accordingly, the shift of the SrTiO_3 XRD peaks is attributed to the incorporation of hydroxyl groups in the SrTiO_3 crystals.

Secondary electron images, obtained by a scanning transmission electron microscope (STEM), of these hybrid particles synthesized from the gels with molar ratios of Ag:Sr:Ti = 1:0:4–1:3:4 via the hydrothermal treatment are shown in Figure 4. The synthesized Ag- SrTiO_3 hybrid particles have a dendritic structure consisting of many branched nanoparticles. The particle size of the particles is sub-micro- to micro-meter order, and the particle size decreases with the Sr molar fraction in the precursor gels. The formation of the particles with similar hierarchical structures was reported for the other perovskite compounds. Maxim *et al.* [25] reported the hydrothermal synthesis of the dendritic

BaTiO₃ particles by using layered titanate as a precursor. Daniels *et al.* [26] reported dendritic La_{0.5}Sm_{0.5}CrO₃ particles synthesized by the sol-gel-hydrothermal method. Other research groups reported the synthesis of single-crystal BaTiO₃ [27], Ba_{1-x}Sr_xTiO₃ [28] and SrTiO₃ dendrites [29]. We have also reported dendritic Ag-BaTiO₃ hybrid particles by using the gels derived by the sol-gel process [15]. Such dendritic growth is promoted under the non-equilibrium condition, in which the growth rate of crystals sufficiently exceeds the mass transport rate of ions for the crystal growth (diffusion-limited aggregation phenomena) [25,27,29–32]. In our present study, we consider that the formation mechanism of the dendritic hybrid nanoparticles is explained by an analogy to these dendritic perovskite particles. During hydrothermal treatment, the amorphous titanium oxide gels with Ag⁺ and Sr²⁺ ions are locally dissolved in basic solutions, and SrTiO₃ nuclei immediately form by the reaction of the dissolved titanium oxide gels with Sr²⁺ ions in the reaction solution and/or in the dried gel itself. As the sol-gel-derived amorphous titanium oxide gels can be considered to act as highly reactive precursors, the nucleation rate of SrTiO₃ is fast, and a large amount of nuclei is formed in the reaction solution [22]. The high surface tension anisotropy induced in the nuclei, owing to a large number of defects, gives rise to dendritic growth in the diffusion-limited aggregation phenomena [25]. On the other hand, the dissolution of the precursor gels is accompanied by a release of Ag⁺ ions. Thus, the local concentration of Ag⁺ ions around the growing SrTiO₃ dendrites increases, and these Ag⁺ ions react with OH⁻ ions and immediately form nanocrystalline precipitates on the surface of SrTiO₃ dendrites. Ag₂O is expected to be formed in basic aqueous solutions at room temperature, but Ag₂O is then reduced under the hydrothermal conditions [15]. As a result of competitive formation reactions of Ag and SrTiO₃ around the precursor gels, Ag nanoparticle-loaded SrTiO₃ hybrid nanoparticles can be obtained.

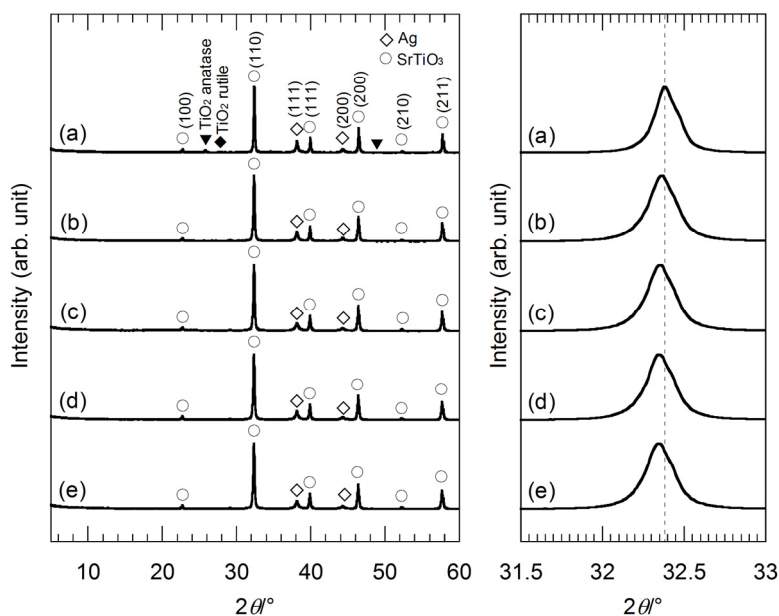


Figure 2. (Left) XRD patterns of the hybrid particles synthesized from the precursor gels with molar ratios of (a) Ag:Sr:Ti = 1:0:4; (b) 1:1:4; (c) 1:2:4; (d) 1:3:4 and (e) 1:4:4 by the hydrothermal treatment at 230 °C for 6 h in Sr(OH)₂ aqueous solutions. (Right) XRD peaks of the hybrid particles indexed as (110) of SrTiO₃ in the 2θ range of 31.5°–33.0°. The slight peak-shift can be clearly seen.

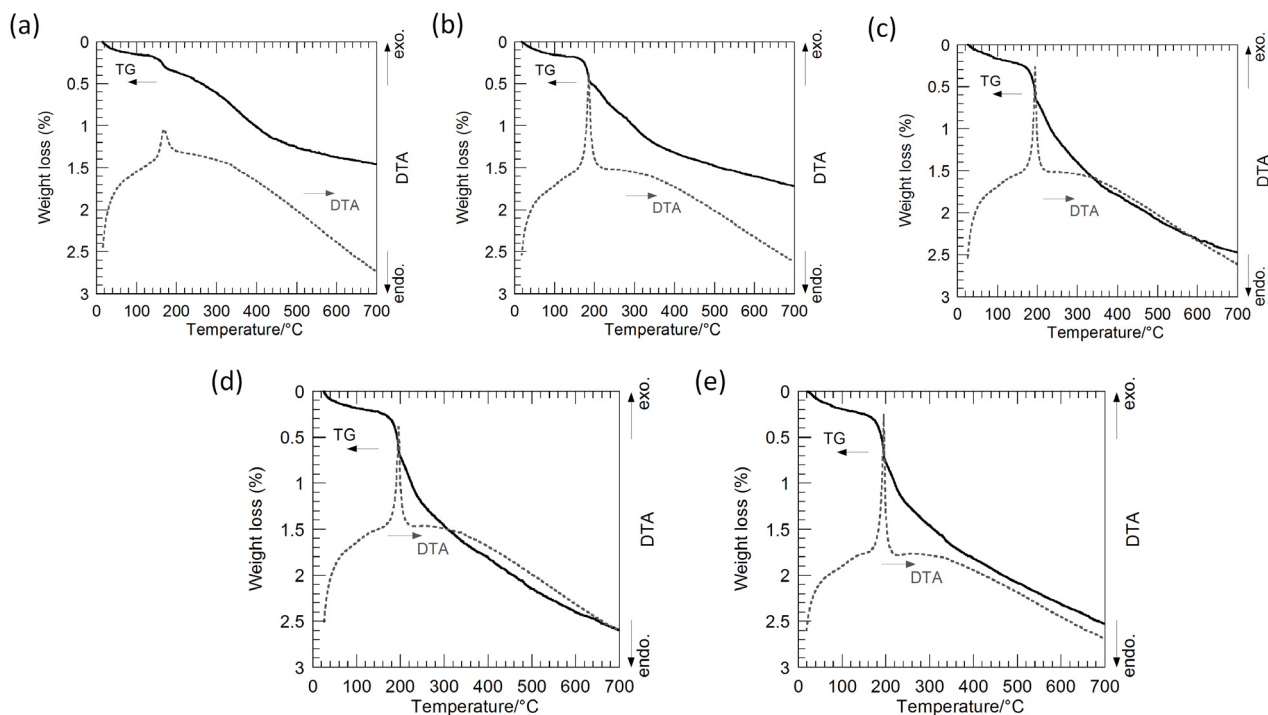


Figure 3. Thermogravimetry-differential thermal analysis (TG-DTA) curves of the Ag-SrTiO₃ hybrid particles synthesized from the precursor gels with molar ratios of (a) Ag:Sr:Ti = 1:0:4; (b) 1:1:4; (c) 1:2:4; (d) 1:3:4; and (e) 1:4:4 by the hydrothermal treatment at 230 °C for 6 h in Sr(OH)₂ aqueous solutions.

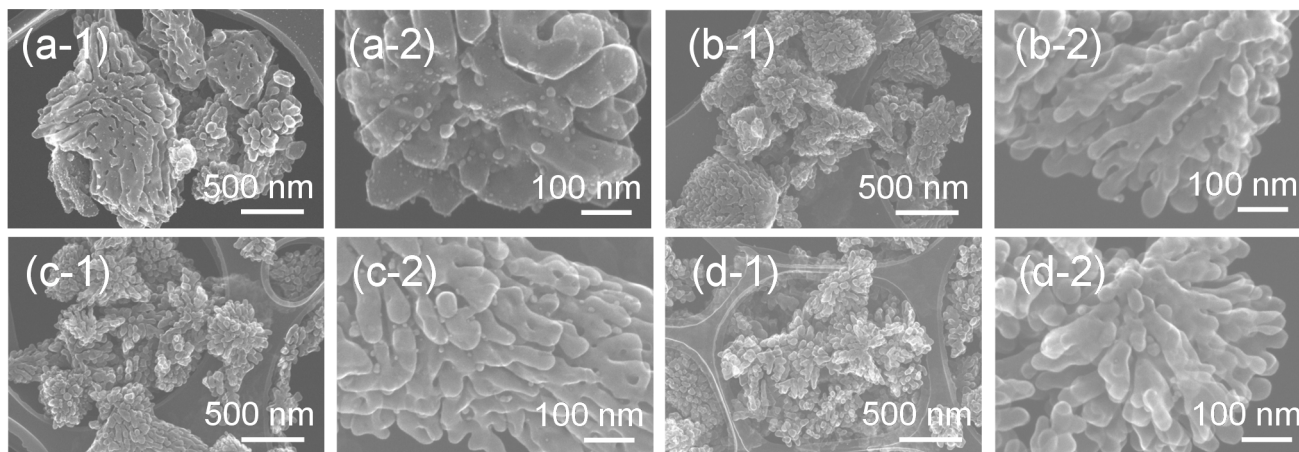


Figure 4. Secondary electron images of the Ag-SrTiO₃ hybrid particles synthesized from the gels with a molar ratio of (a) Ag:Sr:Ti = 1:0:4, (b) 1:1:4, (c) 1:2:4 and (d) 1:3:4 by the hydrothermal treatment at 230 °C for 6 h in Sr(OH)₂ aqueous solutions obtained by the STEM at (a-1–d-1) low and (a-2–d-2) high magnifications.

2.3. Synthesis of Hybrid Particles from Precursor Gels with Various Ag Molar Fractions

Figure 5 shows the XRD patterns of the hybrid particles synthesized from the precursor gels with molar ratios of Ag:Sr:Ti = 0:4:4, 1:4:4, 2:4:4 and 4:4:4 by the hydrothermal treatment at 230 °C for 6 h in Sr(OH)₂ aqueous solutions. All of the XRD peaks are identified as Ag and SrTiO₃, suggesting

the formation of the Ag-SrTiO₃ hybrid particles. The broadness of the XRD peaks originating from Ag is almost the same for all the hybrid particles, and thus, the crystalline size of the Ag nanoparticles is assumed to be similar. In Figure 5, the shift of the XRD peaks of the hybrid particles indexed as (110) of SrTiO₃ in the 2θ range of 31.5°–33.0° is not found. The XRD peak-shift is related to the Sr molar fractions in the precursor gels.

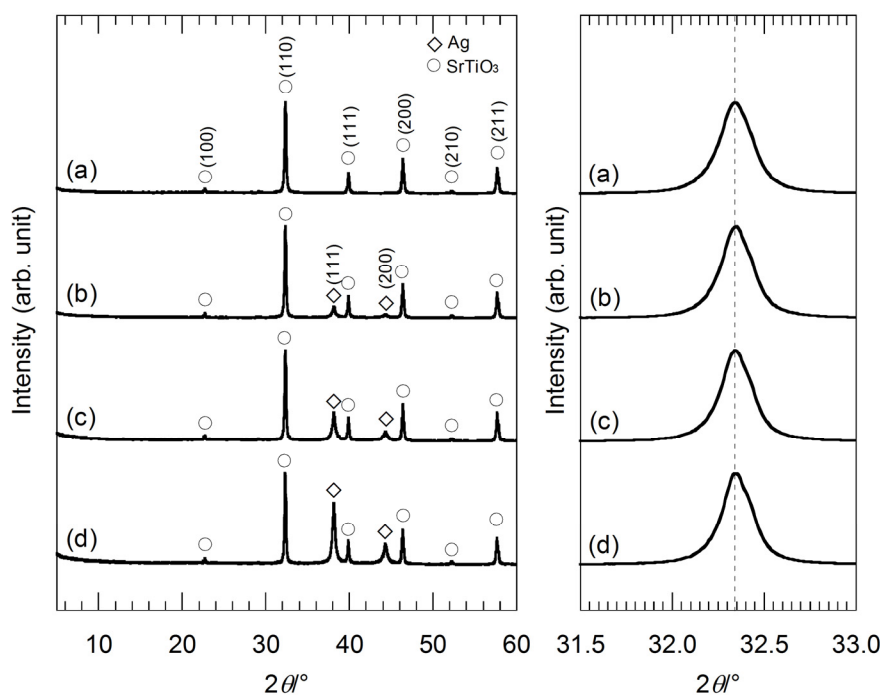


Figure 5. (Left) XRD patterns of the hybrid particles synthesized from the precursor gels with molar ratios of (a) Ag:Sr:Ti = 0:4:4; (b) 1:4:4; (c) 2:4:4; and (d) 4:4:4 by the hydrothermal treatment at 230 °C for 6 h in Sr(OH)₂ aqueous solutions; (Right) XRD peaks of the hybrid particles indexed as (110) of SrTiO₃ in the 2θ range of 31.5°–33.0°.

Figure 6 shows the TG-DTA curves of these hybrid particles synthesized from the precursor gels with the various Ag molar fractions, and a weight loss of 2.2%–2.6% up to 700 °C is found for all the hybrid particles. The sharp exothermic peaks appear at around 180 °C in the DTA curves of the Ag-SrTiO₃ hybrid particles, while such exothermic peaks cannot be found for the SrTiO₃ particles without Ag. Accordingly, it is suggested that the precursor gels were almost completely converted into Ag and SrTiO₃ by the hydrothermal treatment at 230 °C for 6 h in Sr(OH)₂ solutions, but a small amount of the hydroxyl groups might be present. The slightly large weight loss of around 1.7%–2.0% in the range from 200 to 700 °C, which may be attributed to the hydroxyl ions incorporated in the SrTiO₃ crystals, is found for these SrTiO₃ and Ag-SrTiO₃ hybrid particles synthesized from the gels with molar ratios of Ag:Sr:Ti = 0:4:4, 1:4:4, 2:4:4 and 4:4:4 at 230 °C for 6 h in Sr(OH)₂ aqueous solutions. It is considered that these hydroxyl defects induce the enlargement of the SrTiO₃ lattices and result in the XRD peak-shift toward a lower 2θ angle (Figure 5a–d) as compared to the hybrid particles from the precursor gel without Sr²⁺ ions (Figure 2a).

Figure 7a,b shows a secondary electron image obtained by the STEM and field-emission transmission electron microscope (FE-TEM) images of the SrTiO₃ particles synthesized from the gel

with the molar ratio of Ag:Sr:Ti = 0:4:4 at 230 °C for 6 h in Sr(OH)₂ solutions, respectively. It can be clearly seen that dendritic nanoparticles with a size of a few hundreds of nanometers were formed. The selected-area electron diffraction (SAED) analysis was performed for the dendritic SrTiO₃ particle shown in Figure 7b, and the spot pattern was obtained for the corresponding area (Figure 7c). A dendritic SrTiO₃ particle is not a single crystal, but a part of the branches may have a single-crystalline nature.

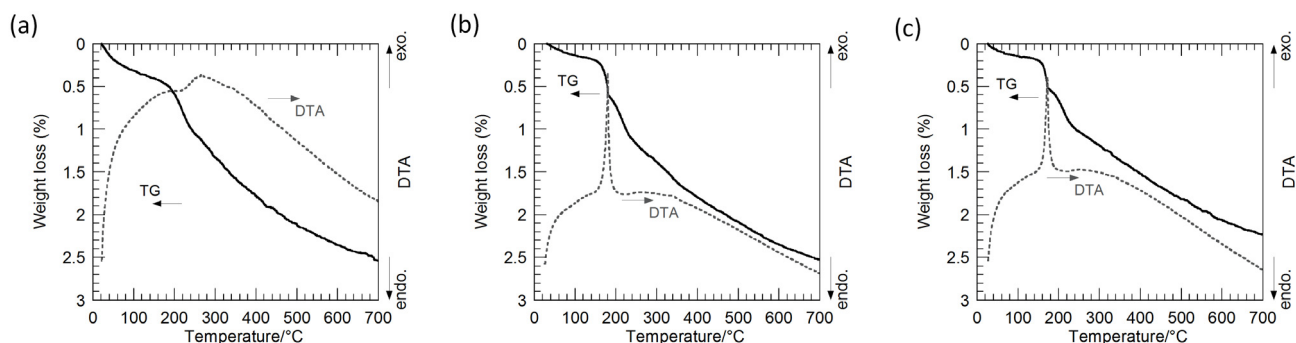


Figure 6. TG-DTA curves of the SrTiO₃ and the Ag-SrTiO₃ hybrid particles synthesized from the precursor gels with molar ratios of Ag:Sr:Ti = (a) 0:4:4; (b) 2:4:4; and (c) 4:4:4 by the hydrothermal treatment at 230 °C for 6 h in Sr(OH)₂ aqueous solutions.

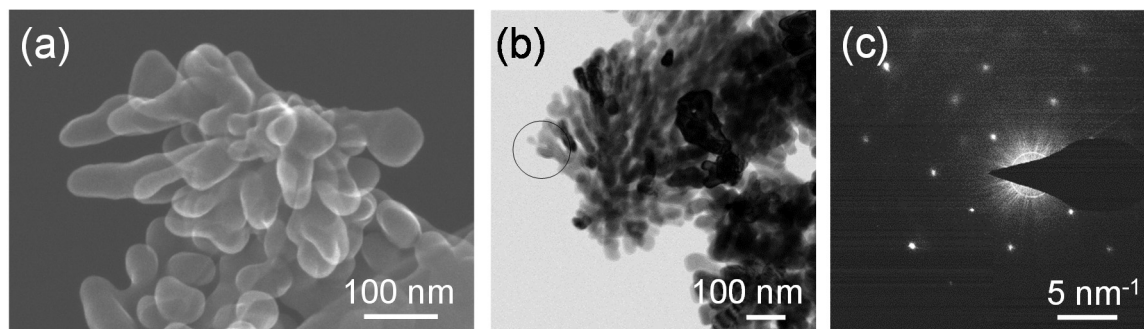


Figure 7. (a) A secondary electron image obtained by the STEM; and (b) Field-emission transmission electron microscope (FE-TEM) images of the SrTiO₃ particles synthesized from the gel with a molar ratio of Ag:Sr:Ti = 0:4:4 by the hydrothermal treatment at 230 °C for 6 h in Sr(OH)₂ aqueous solutions; (c) electron diffraction pattern of the SrTiO₃ particles synthesized from the gels without Ag (the molar ratio of Ag:Sr:Ti = 0:4:4) obtained by the selected area shown in (b).

Figure 8 shows FE-TEM images and the corresponding high-angle annular dark field (HAADF)-STEM images with STEM-energy dispersive X-ray spectroscopy (EDX) mapping of the Ag-SrTiO₃ hybrid particles synthesized from the gels with the various Ag fractions by the hydrothermal treatment at 230 °C for 6 h in Sr(OH)₂ solutions. We can see the Ag nanoparticles are loaded on the SrTiO₃ dendritic nanoparticles, which may have a high specific surface area. There is a wide size distribution of the adsorbed Ag nanoparticles, but the Ag nanoparticles with a size of a few tens of nanometers are distributed without severe agglomeration in these observation areas. By using the sol-gel-derived amorphous titanium oxide gels incorporated with the metal source as the precursors, we could obtain the

Ag nanoparticle-loaded SrTiO₃ dendritic nanoparticles by the hydrothermal treatment at low temperature. These Ag-SrTiO₃ hybrid nanoparticles are expected to be applied to the high-capacitance Ag/SrTiO₃ composite materials or the photocatalysts.

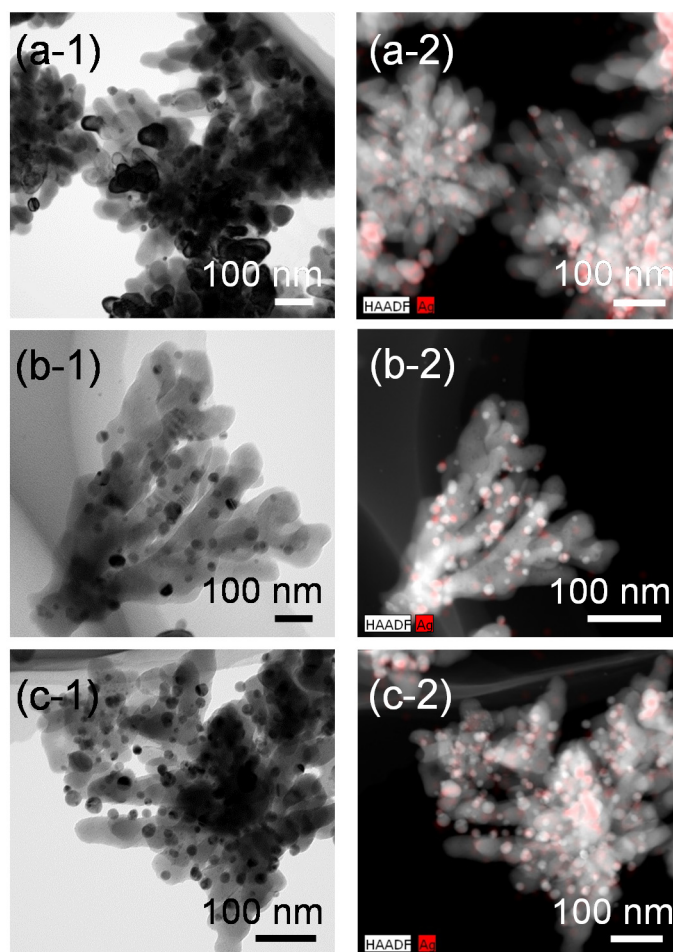


Figure 8. FE-TEM images of the Ag-SrTiO₃ hybrid particles synthesized from the gels with molar ratios of (a-1) Ag:Sr:Ti = 1:4:4; (b-1) 2:4:4 and (c-1) 4:4:4 by the hydrothermal treatment at 230 °C for 6 h in Sr(OH)₂ aqueous solutions. (a-2–c-2) Corresponding high-angle annular dark field (HAADF)-STEM images with STEM-energy dispersive X-ray spectroscopy (EDX) mapping of the hybrid particles shown in (a-1–c-1), respectively. Red-colored regions correspond to the Ag nanoparticles.

3. Experimental Section

The precursor gels were prepared by the conventional sol-gel process. Twelve point five millimolar per decimeter cubed of CH₃COOAg (Wako Pure Chemical, 97.0%, Osaka, Japan) and 0, 12.5, 25, 37.5 and 50 mmol/dm³ Sr(CH₃COO)₂·0.5 H₂O (Wako Pure Chemical, 99.0%) were completely dissolved in 15 mL of deionized water at 80 °C. On the other hand, 50 mmol/dm³ Ti[(CH₃)₂CHO]₄ (Wako Pure Chemical, 95.0%) and 100 mmol/dm³ acetyl acetone (CH₃COCH₂COCH₃, Wako Pure Chemical, 99.0%) were mixed with 15 mL of ethanol. Then, these aqueous and ethanolic solutions were completely mixed, and homogeneous solutions with various Sr molar fractions (molar ratios of Ag:Sr:Ti = 1:0:4, 1:1:4, 1:2:4, 1:3:4 and 1:4:4) were prepared.

We carried out another set of experiments in which we changed the concentration of CH_3COOAg for the aqueous solutions; 0, 12.5, 25, 37.5 and 50 mmol/dm^3 CH_3COOAg and 50 mmol/dm^3 $\text{Sr}(\text{CH}_3\text{COO})_2 \cdot 0.5\text{H}_2\text{O}$ were completely dissolved in 15 mL of deionized water at 80 °C. These aqueous solutions were mixed with 15 mL of 50 mmol/dm^3 $\text{Ti}[(\text{CH}_3)_2\text{CHO}]_4$ and 100 mmol/dm^3 $\text{CH}_3\text{COCH}_2\text{COCH}_3$ ethanolic solutions and were turned into homogeneous solutions with various Ag molar fractions (molar ratios of Ag:Sr:Ti = 0:4:4, 2:4:4 and 4:4:4). After these mixed solutions were dried at 120 °C, these gels were ground into powders, and the precursor gels were obtained.

One hundred milligrams of the precursor gels were added to 10 mL of the strontium hydroxide octahydrate ($\text{Sr}(\text{OH})_2 \cdot 8\text{H}_2\text{O}$, Wako Pure Chemical, 90.0%) aqueous solution with a concentration of 75 mmol/dm^3 . Then, the hydrothermal treatment was performed at 230 °C for 6 h with a heating rate of 5 °C/min in an autoclave. The resultant powders were washed with 3 vol% of formic acid aqueous solution and were dried at 80 °C.

The crystal structure of the samples was identified by XRD measurement using Cu $K\alpha$ radiation (Ultima IV, Rigaku Co., Tokyo, Japan). The thermal decomposition behavior of the precursor gel was examined by TG-DTA (DTG-60, Shimadzu, Kyoto, Japan) performed with a heating rate of 10 °C/min in air. Microstructures of the sample powders were observed by STEM (HD-2300C, Hitachi High-Technologies, Hitachi, Japan) equipped with a secondary electron detector and a field-emission transmission electron microscope (FE-TEM; Osiris, FEI, Hillsboro, OR, USA) equipped with EDX.

4. Conclusions

The Ag nanoparticle-loaded SrTiO_3 nanoparticles were successfully synthesized from the titanium oxide gels incorporated with Ag^+ ions by the sol-gel-hydrothermal method at 230 °C for 6 h in $\text{Sr}(\text{OH})_2$ aqueous solutions. According to the TG analysis, these hybrid particles contain a small amount of hydroxyl defects. The morphology of the SrTiO_3 nanoparticles is dendritic in the presence and absence of Ag^+ ions. The amorphous titanium oxide gels with Ag^+ and Sr^{2+} ions, which act as the high reactive precursor, give rise to high nucleation and growth rates under the hydrothermal conditions, and the resultant diffusion-limited aggregation phenomena facilitate the dendritic growth of SrTiO_3 . From the FE-TEM observation of these Ag- SrTiO_3 hybrid nanoparticles, the Ag nanoparticles with a size of a few tens of nanometers are distributed without severe agglomeration, owing to the competitive formation reactions of Ag and SrTiO_3 .

Author Contributions

Shintaro Ueno and Satoshi Wada designed the outline of the experiments, and Shintaro Ueno performed the experiments. Kouichi Nakashima analyzed the microstructures of the materials by STEM. Yasunao Sakamoto supported the characterization of the materials by XRD and TG-DTA. All the authors contributed to a interpretation of the experimental results, and Shintaro Ueno wrote the paper.

Conflicts of Interest

The authors declare no conflict of interest.

References

1. Fang, L.M.; Zu, X.T.; Li, Z.J.; Zhu, S.; Liu, C.M.; Zhou, W.L.; Wang, L.M. Synthesis and characteristics of Fe³⁺-doped SnO₂ nanoparticles via sol-gel-calcination or sol-gel-hydrothermal route. *J. Alloys Compd.* **2008**, *454*, 261–267.
2. Li, Z.; Houa, B.; Xu, Y.; Wu, D.; Sun, Y.; Hu, W.; Deng, F. Comparative study of sol-gel-hydrothermal and sol-gel synthesis of titania-silica composite nanoparticles. *J. Solid State Chem.* **2005**, *178*, 1395–1405.
3. Wang, W.; Cao, L.; Liu, W.; Su, G.; Zhang, W. Low-temperature synthesis of BaTiO₃ powders by the sol-gel-hydrothermal method. *Ceram. Int.* **2013**, *39*, 7127–7134.
4. Yang, X.; Ren, Z.; Xu, G.; Chao, C.; Jiang, S.; Deng, S.; Shen, G.; Wei, X.; Han, G. Monodisperse hollow perovskite BaTiO₃ nanostructures prepared by a sol-gel-hydrothermal method. *Ceram. Int.* **2014**, *40*, 9663–9670.
5. Zeng, J.; Lin, C.; Li, J.; Li, K. Low temperature preparation of titanate thin films by a novel sol-gel-hydrothermal method. *Mater. Lett.* **1999**, *38*, 112–115.
6. Fuentes, S.; Zarate, R.A.; Chavez, E.; Muñoz, P.; Díaz-Droguett, D.; Leyton, P. Preparation of SrTiO₃ nanomaterial by a sol-gel-hydrothermal method. *J. Mater. Sci.* **2010**, *45*, 1448–1452.
7. Hou, Y.-D.; Hou, L.; Zhang, T.-T.; Zhu, M.-K.; Wang, H.; Yan, H. (Na_{0.8}K_{0.2})_{0.5}Bi_{0.5}TiO₃ nanowires: Low-temperature sol-gel-hydrothermal synthesis and densification. *J. Am. Ceram. Soc.* **2007**, *90*, 1738–1743.
8. Lee, W.W.; Chung, W.-H.; Huang, W.-S.; Lin, W.-C.; Lin, W.-Y.; Jiang, Y.-R.; Chen, C.-C. Photocatalytic activity and mechanism of nano-cubic barium titanate prepared by a hydrothermal method. *J. Taiwan Inst. Chem. Eng.* **2013**, *44*, 660–669.
9. Huang, S.-T.; Lee, W.-W.; Chang, J.-L.; Huang, W.-S.; Chou, S.-Y.; Chen, C.-C. Hydrothermal synthesis of SrTiO₃ nanocubes: Characterization, photocatalytic activities, and degradation pathway. *J. Taiwan Inst. Chem. Eng.* **2014**, *45*, 1927–1936.
10. Sui, D.; Yin, X.; Dong, H.; Qin, S.; Chen, J.; Jiang, W. Photocatalytically reducing CO₂ to methyl formate in methanol over Ag loaded SrTiO₃ nanocrystal catalysts. *Catal. Lett.* **2012**, *142*, 1202–1210.
11. Puangpetch, T.; Sreethawong, T.; Yoshikawa, S.; Chavadej, S. Hydrogen production from photocatalytic water splitting over mesoporous-assembled SrTiO₃ nanocrystal-based photocatalysts. *J. Mol. Catal. A* **2009**, *312*, 97–106.
12. Sun, Y.; Liu, J.; Li, Z. Design of highly ordered Ag-SrTiO₃ nanotube arrays for photocatalytic degradation of methyl orange. *J. Solid State Chem.* **2011**, *184*, 1924–1930.
13. Subramanian, V.; Roeder, R.K.; Wolf, E.E. Synthesis and UV-visible-light photoactivity of noble-metal-SrTiO₃ composites. *Ind. Eng. Chem. Res.* **2006**, *45*, 2187–2193.
14. Puangpetch, T.; Sreethawong, T.; Chavadej, S. Hydrogen production over metal-loaded mesoporous-assembled SrTiO₃ nanocrystal photocatalysts: Effects of metal type and loading. *Int. J. Hydrog. Energy* **2010**, *35*, 6531–6540.
15. Ueno, S.; Sakamoto, Y.; Nakashima, K.; Wada, S. Microstructure and dielectric properties of silver-barium titanate nanocomplex materials by wet chemical approach. *Jpn. J. Appl. Phys.* **2014**, *53*, 09PB05.

16. Pecharromás, C.; Esteban-Betegón, F.; Bartolomé, J.F.; López-Esteban, S.; Moya, J.S. New percolative BaTiO₃-Ni composites with a high and frequency-independent dielectric constant ($\epsilon_r \approx 80,000$). *Adv. Mater.* **2001**, *13*, 1541–1544.
17. Pecharromás, C.; Moya, J.S. Experimental evidence of a giant capacitance in insulator-conductor composites at the percolation threshold. *Adv. Mater.* **2000**, *12*, 294–297.
18. Chen, Z.; Huang, J.; Chen, Q.; Song, C.; Han, G.; Weng, W.; Du, P. A percolative ferroelectric-metal composite with hybrid dielectric dependence. *Scr. Mater.* **2007**, *57*, 921–924.
19. Huang, J.; Cao, Y.; Hong, M. Ag-Ba_{0.75}Sr_{0.25}TiO₃ composites with excellent dielectric properties. *Appl. Phys. Lett.* **2008**, *92*, 022911.
20. Shannon, R.D.; Prewitt, C.T. Effective ionic radii in oxides and fluorides. *Acta Cryst.* **1969**, *B25*, 925–946.
21. Hennings, D.F.K.; Metzmacher, C.; Schreinemacher, B.S. Defect chemistry and microstructure of hydrothermal barium titanate. *J. Am. Ceram. Soc.* **2001**, *84*, 179–182.
22. Chen, H.; Chen, Y.-W. Hydrothermal synthesis of barium titanate. *Ind. Eng. Chem. Res.* **2003**, *42*, 473–483.
23. Xia, C.-T.; Shi, E.-W.; Zhong, W.-Z.; Guo, J.-K. Preparation of BaTiO₃ by the hydrothermal method. *J. Eur. Ceram. Soc.* **1995**, *15*, 1171–1176.
24. Shi, E.-W.; Xia, C.-T.; Zhong, W.-Z.; Wang, B.-G.; Feng, C.-D. Crystallographic properties of hydrothermal barium titanate crystallites. *J. Am. Ceram. Soc.* **1997**, *80*, 1567–1572.
25. Maxim, F.; Ferreira, P.; Reaney, I. Hydrothermal synthesis and crystal growth studies of BaTiO₃ using Ti nanotube precursors. *Cryst. Growth Des.* **2008**, *8*, 3309–3315.
26. Daniels, L.M.; Weber, M.C.; Lees, M.R.; Guennou, M.; Kashtiban, R.J.; Sloan, J.; Kreisel, J.; Walton, R.I. Structures and magnetism of the rare-earth orthochromite perovskite solid solution La_xSm_{1-x}CrO₃. *Inorg. Chem.* **2013**, *52*, 12161–12169.
27. Wang, Y.; Xu, G.; Yang, L.; Ren, Z.; Wei, X.; Weng, W.; Du, P.; Shen, G.; Han, G. Hydrothermal synthesis of single-crystal BaTiO₃ dendrites. *Mater. Lett.* **2009**, *63*, 239–241.
28. Yang, L.; Wang, Y.; Wang, Y.; Wang, X.; Guo, X.; Han, G. Synthesis of single-crystal Ba_{1-x}Sr_xTiO₃ ($x = 0-1$) dendrites via simple hydrothermal method. *J. Alloys Compd.* **2010**, *500*, L1–L5.
29. Wang, Y.; Xu, G.; Yang, L.; Ren, Z.; Wei, X.; Weng, W.; Du, P.; Shen, G.; Han, G. Formation of single-crystal SrTiO₃ dendritic nanostructures via a simple hydrothermal method. *J. Cryst. Growth* **2009**, *311*, 2519–2523.
30. Matsushita, M.; Sano, M.; Hayakawa, Y.; Honjo, H.; Sawada, Y. Fractal structures of zinc metal leaves grown by electrodeposition. *Phys. Rev. Lett.* **1984**, *53*, 286–289.
31. Oaki, Y.; Imai, H. Experimental demonstration for the morphological evolution of crystals grown in gel media. *Cryst. Growth Des.* **2003**, *3*, 711–716.
32. López, C.M.; Choi, K.-S. Electrochemical synthesis of dendritic zinc films composed of systematically varying motif crystals. *Langmuir* **2006**, *22*, 10625–10629.